Journal of Environmental Chemical Engineering 3 (2015) 852–861

Contents lists available at ScienceDirect

Journal of Environmental Chemical Engineering

journal homepage: www.elsevier.com/locate/jece

In situ growth strategy for highly efficient Ag_2CO_3/g-C_3N_4 hetero/nanojunctions with enhanced photocatalytic activity under sunlight irradiation

Surendar Tonda, Santosh Kumar [1], Vishnu Shanker *

Department of Chemistry, National Institute of Technology Warangal, Warangal,Telangana, 506004 India

ARTICLE INFO

Article history:
Received 13 February 2015
Received in revised form 12 March 2015
Accepted 22 March 2015
Available online 28 March 2015

Keywords:
Heterojunctions
Photocorrosion
Ag_2CO_3
g-C_3N_4
Sunlight
Degradation

ABSTRACT

Developing novel heterojunction photocatalysts is a powerful strategy for improving the separation efficiency of photogenerated charge carriers, which is attracting the intense research interest in photocatalysis. Herein we report a highly efficient hetero/nanojunction consisting of Ag_2CO_3 nanoparticles grown on layered g-C_3N_4 nanosheets synthesized *via* a facile and template free *in situ* precipitation method. The UV–vis diffuse reflectance studies revealed that the synthesized Ag_2CO_3/g-C_3N_4 hetero/nanojunctions exhibit a broader and stronger light absorption in the visible light region, which is highly beneficial for absorbing the visible light in the solar spectrum. The optimum photocatalytic activity of Ag_2CO_3/g-C_3N_4 at a weight content of 10% Ag_2CO_3 for the degradation of Rhodamine B was almost 5.5 and 4 times as high as that of the pure Ag_2CO_3 and g-C_3N_4, respectively. The enhanced photocatalytic activity of the Ag_2CO_3/g-C_3N_4 hetero/nanojunctions is due to synergistic effects including the strong visible light absorption, large specific surface area, and high charge transfer and separation efficiency. More importantly, the high photostability and low use of the noble metal silver which reduces the cost of the material. Therefore, the synthesized Ag_2CO_3/g-C_3N_4 hetero/nanojunction photocatalyst is a promising candidate for energy storage and environment protection applications.

Introduction

Sunlight is an ideal and natural resource of energy and converting sunlight into chemical energy, mimicking what nature does, has been considered as a most promising and sustainable approach to meet the global energy demands and overcome their associated environmental issues [1–3]. So, one of the major scientific challenges of researchers is to target a novel and efficient semiconductor photocatalysts for H_2 generation from water splitting and degradation of organic pollutants in wastewater through photocatalysis. Although traditional semiconductor photocatalysts such as TiO_2 and ZnO have been extensively studied for such a purpose, they exhibit appreciable photocatalytic activity only under UV light (2–4% of the solar spectrum), which greatly limits the practical application for solar energy conversion [4,5]. Therefore, the current research in the field of photocatalysis mainly focuses on search for active photocatalytic materials with band gap corresponding to the energy of visible light for efficient utilization of sunlight.

To date, a series of visible light responsive photocatalysts have been reported. In particular, silver-based semiconductors, among numerous photocatalysts, have attracted much attention for their high visible light activity [6–8]. Yi et al. reported a novel Ag_3PO_4 photocatalyst with enhanced photocatalytic activity for water splitting and decomposition of organic contaminants under visible light irradiation [9]. However, Ag_3PO_4 readily decomposes photochemically if no sacrificial reagent is involved. Kato et al. reported that $AgNbO_3$ exhibits high photocatalytic activity for H_2 evolution from water splitting under visible-light irradiation in the presence of sacrificial reagents [10]. Hu et al. reported a monoclinic Ag_3VO_4 with enhanced visible light photocatalytic activity for the degradation of organic pollutant acid red B [11]. As a new silver-based semiconductor photocatalyst, Ag_2CO_3 has been reported to exhibit highly efficient degradation capability for various organic pollutants including Rhodamine B, methylene blue and methyl orange [12,13]. Unfortunately, the aforementioned silver-based photocatalysts are photochemically unstable because they readily undergo photo-corrosion during photocatalysis process, which can seriously deactivate the photocatalysts. Dai et al. investigated that the photo-corrosion of Ag_2CO_3 could be efficiently inhibited by

* Corresponding author. Tel.: +91 870 2462675; fax: +91 870 2459547.
E-mail address: vishnu@nitw.ac.in (V. Shanker).
[1] Present address: European Bioenergy Research Institute, Aston University, Birmingham, B4 7ET, UK.

http://dx.doi.org/10.1016/j.jece.2015.03.021
2213-3437/

using silver nitrate as an electron acceptor in the photocatalytic process [14]. Very recently, Yu et al. reported that Ag_2O/Ag_2CO_3 heterostructure exhibited much higher photocatalytic activity and stability than the pure Ag_2CO_3 [15]. In this sense, the promotion of the photocatalytic activity and stability become an urgent task for these silver-based semiconductor photocatalysts.

Recently, an organic and metal-free polymeric graphitic carbon nitride (g-C_3N_4), which is the most stable allotrope of all carbon nitride materials under ambient conditions, has attracted considerable attention due to its unique properties such as thermal stability, reliable chemical inertness, non-toxicity, easy modification and outstanding electrical property [16,17]. As a new class of polymeric visible light driven photocatalysts with suitable band gap (2.7 eV), g-C_3N_4 can be easily synthesized *via* one step polycondensation of cheap and easily available precursors like melamine, urea, thiourea, cyanamide and dicyanamide [17–19]. Owing to its special properties, g-C_3N_4 has been explored as a "sustainable" photocatalyst, which exhibits high photocatalytic performance for photo-electrochemical conversion, hydrogen generation from water splitting and degradation of organic pollutants under visible light irradiation [20]. Nevertheless, the relatively low quantum efficiency of pure g-C_3N_4 still limits its practical application due to the high recombination rate of photogenerated electron–hole pairs and low specific surface area [20,21]. To resolve this problem, many attempts have been made to improve the photocatalytic performance of g-C_3N_4, such as combining with conductive materials (graphene, CNTs) for faster charge transfer, constructing heterojunction with other semiconductors (Ag_3PO_4, ZnO, Fe_3O_4) for effective charge separation, or loading cocatalysts (Au, Fe) to trap the photo-excited electrons [21–27].

Construction of semiconductor heterojunctions by combining two different catalysts with suitable conduction and valence bands is one of the effective approaches to enhance the generation and separation efficiency of photo-induced electron–hole pairs during the photocatalytic process [28,29]. It is well accepted that interface properties of heterojunctions are critical for determining the final photocatalytic activity of the system. In general, interface properties can be attributed to two important aspects. First, the lattice match between the two components, which is the essential for fabricating semiconductor heterojunctions and the other, is the suitable valence and conduction band levels, considered to be the foremost and fundamental requirement for charge transfer and separation at the hetero-structured interfaces [28,30].

Inspired from this, we report the fabrication of hetero/nanojunction between Ag_2CO_3 nanoparticles (NPs) and g-C_3N_4 nanosheets *via* a facile and template free *in situ* growth fabrication method for improved charge transfer and separation at the hetero/nanojunction interface. Interestingly, the Ag_2CO_3/g-C_3N_4 hetero/nanojunctions exhibit a remarkably enhanced photocatalytic performance for the degradation of Rhodamine B and 4-chlorophenol under sunlight irradiation. Moreover, the kinetics and the possible photocatalytic mechanism of the Ag_2CO_3/g-C_3N_4 hetero/nanojunction related to the band positions of the two semiconductors were also discussed in detail. However, the reports on g-C_3N_4/Ag_2CO_3 composite materials for other groups which only focus on formation of bulk heterostructure of g-C_3N_4/Ag_2CO_3 with poor interface at the heterojunction and low surface area [31,32]. Unfortunately, in these reports a small amount of g-C_3N_4 being introduced on Ag_2CO_3 material, which made them as Ag_2CO_3-based materials, resulting in high usage of the noble metal. In the present study, we focus on g-C_3N_4 nanosheet of high surface area based materials by forming a heterostructure with minimum amount of Ag_2CO_3 and maximum activity which significantly reduces the use of the noble metal silver, thereby effectively reducing the cost of the material. Therefore, the better heterostructure of low noble metal based material with high surface area showed an improved photocatalytic performance over these reports from the literature.

Experimental

Materials

Silver nitrate (99.9%), Rhodamine B (95.0%) and Melamine (99.0%) were purchased from Sigma–Aldrich. Sodium bicarbonate (99.5%) and 4-chlorophenol (98%) were obtained from Sisco Research Laboratories Pvt., Ltd., Ammonium oxalate, terephthalic acid, and tert-butyl alcohol were analytically pure and purchased from Merck chemicals. All other reagents were used without further purification.

Method

Synthesis of g-C_3N_4 nanosheets

The pure g-C_3N_4 nanosheets were synthesized according to a procedure described in our previous paper [27]. Briefly, melamine was placed in an alumina boat and heated at 550 °C for 2 h under a N_2 atmosphere with a slow ramp rate to get a bulk g-C_3N_4. Then the bulk g-C_3N_4 was subjected to a liquid exfoliation in water to synthesize g-C_3N_4 nanosheets. In detail, 0.1 g of bulk g-C_3N_4 powder was dispersed in 250 mL water and then ultrasonicated overnight. The formed suspension was heated at 100 °C to remove water and the resulting pale yellow colored g-C_3N_4 nanosheets are denoted as CN.

Synthesis of Ag_2CO_3 nanoparticles

The Ag_2CO_3 sample was synthesized by a simple ion exchange method. In a typical procedure, 40 mL of silver nitrate aqueous solution (0.1 M) was placed in a beaker and an aqueous solution of sodium bicarbonate (0.05 M) was added dropwise under stirring condition at room temperature. After continuous stirring for 24 h, the obtained yellowish green precipitation was collected by centrifugation and washed with double distilled water followed by ethanol for several times. Then the product was dried in an oven at 80 °C for 2 h and the resultant Ag_2CO_3 sample was named as AGCO.

Synthesis of Ag_2CO_3/g-C_3N_4 hetero/nanojunction

For the synthesis of the Ag_2CO_3/g-C_3N_4 hetero/nanojunction, we have employed an *in situ* growth strategy. In a typical procedure, an appropriate amount of g-C_3N_4 nanosheets was ultrasonicated in 50 mL of water for 2 h. To this suspension, 0.85 g of silver nitrate was added and stirred for 30 min at room temperature. Subsequently, 50 mL of 0.05 M sodium bicarbonate aqueous solution was added dropwise and stirred for 24 h. The obtained precipitation was centrifuged, washed with water and ethanol and finally dried at 80 °C for 2 h. A series of Ag_2CO_3/g-C_3N_4 hetero/nanojunctions were synthesized with different weight ratios of Ag_2CO_3 and 5, 10 and 20 wt% Ag_2CO_3 samples are denoted as AGCOCN-5, AGCOCN-10 and AGCOCN-20, respectively.

Material characterization

X-ray diffraction (XRD) measurements were recorded at room temperature using a Bruker AXS D8 Advance X-ray diffractometer with Ni filtered Cu Kα radiation (λ = 1.5406 Å). Zeta-potential measurements were carried out on a Malvern Zetasizer NANO ZS analyzer. Fourier transform infrared (FT-IR) spectra were conducted using a PerkinElmer Spectrum 100 FT-IR spectrophotometer in the frequency range 4000–400 cm^{-1} with a resolution of 4 cm^{-1}. The diffuse reflectance absorption spectra (DRS) of the

samples were recorded in the range from 220 to 800 nm using a THERMO Scientific Evolution 600 diffuse reflectance spectrophotometer equipped with an integrated sphere, and $BaSO_4$ was used as a reference. Transmission electron microscopy (TEM) measurements were made on a JEOL JSM-6700F transmission electron microscope with an accelerating applied potential of 200 kV. The elemental composition of the samples was analyzed using an energy dispersive spectrometer (EDS) (OXFORD Instruments, INCAx-act). The Brunauer–Emmett–Teller (BET) surface area and pore volume were measured on a Quanta chrome NOVA 1200e analyzer at liquid nitrogen temperature. The photoluminescence (PL) measurements were conducted using a TSC Solutions F96pro fluorescence spectrophotometer with an excitation wavelength of 365 nm.

Evaluation of photocatalytic activity

Rhodamine B (RhB), a widely used dye, was selected as a representative colored pollutant and 4-chlorophenol (4-CP) as a colorless model pollutant to examine the photocatalytic activity of the synthesized samples under sunlight irradiation. The sunlight driven photocatalytic experiments of the synthesized samples were conducted in June 2014 at NIT Warangal, where the fluctuation of the sunlight intensity is minimal during this month. In a typical procedure, an aqueous solution of RhB or 4-CP (250 mL, 5 mg L^{-1}) was placed in a reaction vessel, and then 0.1 g of photocatalyst was added. Prior to irradiation, the suspensions were agitated in the dark for 30 min to ensure adsorption-desorption equilibrium at room temperature. During the irradiation, about 5 mL of the suspension was periodically withdrawn from the reaction cell at given time intervals, and then centrifuged to remove the photocatalyst. Subsequently, the solutions were analyzed by recording variations at the wavelength of maximal absorption in the UV–vis spectrophotometer. A blank test was also conducted on an aqueous RhB or 4-CP solution without catalyst under sunlight irradiation, *i.e.*, photolysis of RhB, to explore the degradation efficiency of the photocatalyst.

Analysis of reactive species

The effect of reactive species on the degradation of RhB over Ag_2CO_3/g-C_3N_4 photocatalysts was examined to understand the photocatalytic reaction mechanism. The detection process for reactive species was similar to the photocatalytic degradation process. However, prior to addition of photocatalyst, suitable scavenger was added to the RhB aqueous solution. Moreover, the generation of hydroxyl radicals ($^{\bullet}OH$) on the surface of sunlight irradiated photocatalyst was examined by the PL technique using terephthalic acid (TA) as a probe molecule. The $^{\bullet}OH$ generated in the system can readily react with TA and produce 2-hydroxyterephthalic acid (TAOH), the PL intensity of which is directly proportional to the generated $^{\bullet}OH$ [33]. In a brief experimental procedure, 0.1 g of Ag_2CO_3/g-C_3N_4 catalyst was dispersed in 100 mL of a mixture of a 5×10^{-4} mol L^{-1} aqueous TA solution and a 2×10^{-3} mol L^{-1} NaOH solution. Then, the resulting suspension was magnetically stirred and exposed to sunlight. At every 5 min intervals, the suspension was collected and centrifuged to measure the maximum PL intensity using fluorescence spectrophotometer with an excitation wavelength of 365 nm.

Electrochemical impedance spectroscopy (EIS) and photocurrent measurements

EIS and photocurrent measurements of the synthesized photocatalysts were performed in a three electrode quartz cell system using an electrochemical workstation (Model: IM6e, ZAHNER, GmbH, Germany). Platinum wire was used as the counter electrode and Ag/AgCl (3 N KCl) electrode used as the reference electrode. The synthesized photocatalyst was served as the working electrode. EIS experiments were conducted at an open circuit potential over the frequency range between 10 mHz and 100 kHz with a sinusoidal ac perturbation of ±5 mV and 10 mM $K_3[Fe(CN)_6]$ containing 0.1 M KCl solution was used as the electrolyte. The photocurrent response of the photocatalysts was investigated for several on–off cycles of irradiation by an Xe arc lamp through a UV-cutoff filter. Na_2SO_4 (0.01 mol L^{-1}) aqueous solution was used as the electrolyte. The preparation procedure of working electrodes was as follows: 10 mg of the synthesized photocatalyst was mixed with 1 mL of double distilled water to make slurry. Then, the obtained slurry was dripped into an indium tin oxide (ITO) glass with 1 cm × 0.5 cm area. Finally, the electrode was dried at 120 °C for 1 h.

Results and discussion

In situ growth strategy

In the present work, we report an *in situ* growth strategy for the synthesis of Ag_2CO_3/g-C_3N_4 hetero/nanojunctions, which is widely used to synthesize a variety of graphene based composites and other organic–inorganic based hetero/nanojunctions [25,34]. Silver nitrate was used as a precursor for Ag_2CO_3. At the early stage of the reaction process, silver nitrate was mixed with ultrasonically dispersed g-C_3N_4 nanosheets and silver ions from the silver salt were strongly bound to the g-C_3N_4 nanosheets *via* electrostatic interactions as shown in Scheme 1. Furthermore, silver ions were converted into Ag_2CO_3 NPs due to ion exchange process after the addition of sodium bicarbonate as a precipitating agent at room temperature. To minimize the surface energy, the synthesized Ag_2CO_3 NPs led the hetero/nanojunction at the interface of the g-C_3N_4 and Ag_2CO_3 in the resulting composite system. Consequently, a strong hetero/nanojunction was successfully constructed between Ag_2CO_3 NPs and g-C_3N_4 nanosheets *via* electrostatic interactions. However, these electrostatic interactions were confirmed from a shift in the zeta-potential of g-C_3N_4 dispersions in water after the formation of hetero/nanojunction with Ag_2CO_3 from negative to positive surface charges from −28.2 to +30.5 mV (Fig. S1).

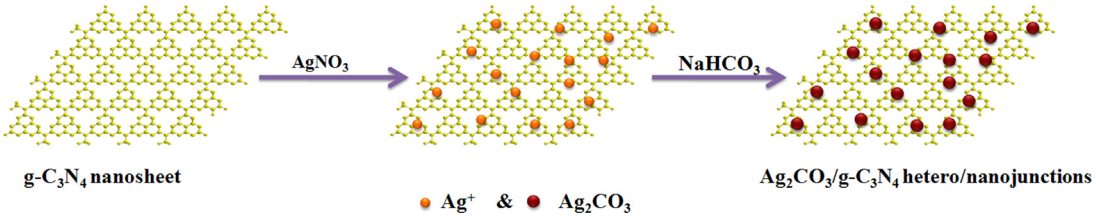

Scheme 1. Schematic representation of the *in situ* deposition of Ag_2CO_3 NPs on a g-C_3N_4 nanosheet.

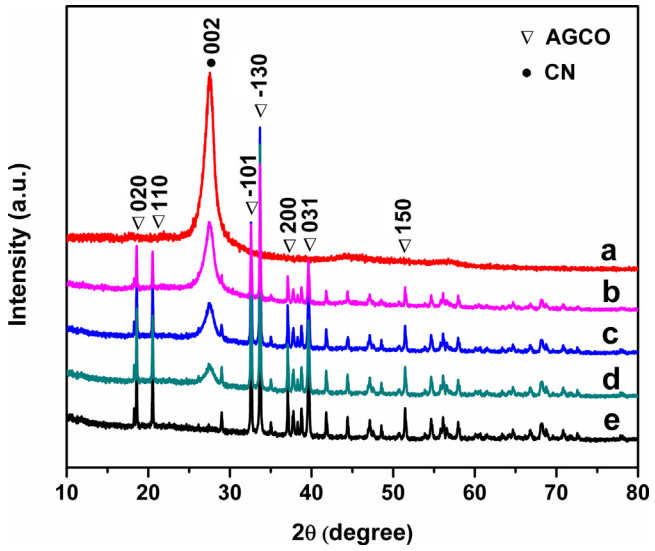

Fig. 1. XRD patterns of the synthesized pure Ag_2CO_3, g-C_3N_4 nanosheets and Ag_2CO_3/g-C_3N_4 hetero/nanojunctions: (a) CN, (b) AGCOCN-5, (c) AGCOCN-10, (d) AGCOCN-20 and (e) AGCO.

Characterizations of the Ag_2CO_3/g-C_3N_4 hetero/nanojunctions

XRD studies were carried out to investigate the phase structure and crystalline nature of the synthesized samples. The results (as shown in Fig. 1.) indicate that the diffraction peak at 27.5°, which is indexed as 002 plane in pure g-C_3N_4 and Ag_2CO_3/g-C_3N_4 samples is due to the interlayer stacking of the conjugated aromatic systems, corresponding to an interlayer distance of $d = 0.332$ nm [26,35]. The pure Ag_2CO_3 displays sharp diffraction peaks at 2θ values of 18.56°, 20.54°, 32.61°, 33.67°, 37.08°, 39.59° and 51.38° correspond to the planes of 020, 110, −101, −130, 200, 031 and 150, respectively, which can be indexed to the monoclinic phase of Ag_2CO_3 (JCPDS No. 26-0339). Moreover, no impurity peaks are detected, indicating the formation of pure monoclinic structure Ag_2CO_3. The sharp and intense diffraction peaks also indicates the good crystalline nature of Ag_2CO_3. The XRD patterns for Ag_2CO_3/g-C_3N_4 samples exhibited diffraction peaks corresponding to both Ag_2CO_3 and g-C_3N_4, reflecting the existence of two phases.

The UV–vis DRS was performed to justify the light harvesting ability of the synthesized samples before and after the formation of the hetero/nanojunction. As shown in Fig. 2a, the synthesized pure Ag_2CO_3 has an absorption edge at around 540 nm. The high visible light absorption of Ag_2CO_3 results from intrinsic transition between the valence band and the conduction band, rather than the transition from the impurity to the conduction band [14]. The pure g-C_3N_4 sample shows photo-absorption in the UV and visible-light regions, and the wavelength of the absorption edge is 465 nm. More interestingly, the absorption intensities of all the Ag_2CO_3/g-C_3N_4 hetero/nanojunctions were shown a significant enhancement at the wavelength range of 450–800 nm compared with g-C_3N_4 and Ag_2CO_3. These results clearly demonstrating that the bonding interaction can effectively decrease the contact barrier and strengthen the electronic coupling of g-C_3N_4 and Ag_2CO_3, leading to the strong light absorption of Ag_2CO_3/g-C_3N_4 hetero/nanojunctions at longer wavelengths. The band gap energies of AGCO, CN and AGCOCN-10 were calculated to be 2.32, 2.75 and 2.15 eV, respectively, according to the Kubelka–Munk functions against the photon energy. The decreased energy gaps of the hetero/nanojunctions reveal the enhanced visible light absorption and thus result in the generation of more photogenerated electron–hole pairs under sunlight irradiation, which subsequently leads to a higher photocatalytic activity [24,36].

Fig. 2b shows the FT-IR spectra of the synthesized pure Ag_2CO_3, g-C_3N_4 nanosheets, and Ag_2CO_3/g-C_3N_4 hetero/nanojunctions. The representative absorption bands of pure g-C_3N_4 could be found at 1571, 1415, 1326 and 1244 cm^{-1} are assigned to the stretching modes of aromatic C—N heterocycles, and the broad absorption band at 3170 cm^{-1} corresponds to the stretching vibrational modes of residual N—H components associated with uncondensed amino groups [27,37]. Additionally, the sharp characteristic peak at 808 cm^{-1} originates from *s*-triazine ring system. For pure Ag_2CO_3, the peaks appearing at 1386 and 887 cm^{-1} are attributed to the characteristic absorption bands of CO_3^{2-} [38]. Moreover, the broad absorption bands observed in all the samples in the range 2800–3450 cm^{-1} correspond to the stretching vibrations of O—H groups in the physically adsorbed H_2O molecules. Nevertheless, the FT-IR spectra of Ag_2CO_3/g-C_3N_4 hetero/nanojunctions are similar to those of the main peaks of pure g-C_3N_4 and Ag_2CO_3 as shown in Fig. 2b . Interestingly, the absorption bands of Ag_2CO_3/g-C_3N_4 hetero/nanojunctions are shifted to a lower wavenumber, and the intensity of these absorption bands was slightly decreases in Ag_2CO_3/g-C_3N_4 hetero/nanojunctions. This phenomenon suggests the strong interactions between Ag_2CO_3 and g-C_3N_4 nanosheets in Ag_2CO_3/g-C_3N_4 hetero/nanojunction system. Based on the above observations, it can be confirmed that Ag_2CO_3/g-C_3N_4 hetero/nanojunction with close interfacial connections between g-C_3N_4 and Ag_2CO_3 was achieved, and these connections may serve as electron migration paths to promote the charge separation, and induce a synergistic effect for an improved photocatalytic activity [39].

The morphology and surface structure of the synthesized Ag_2CO_3/g-C_3N_4 hetero/nanojunctions were investigated by TEM analysis. As shown in Fig. 3(a) and (b), AGCOCN-10 sample exhibited a porous sheet like morphology. Interestingly, Ag_2CO_3

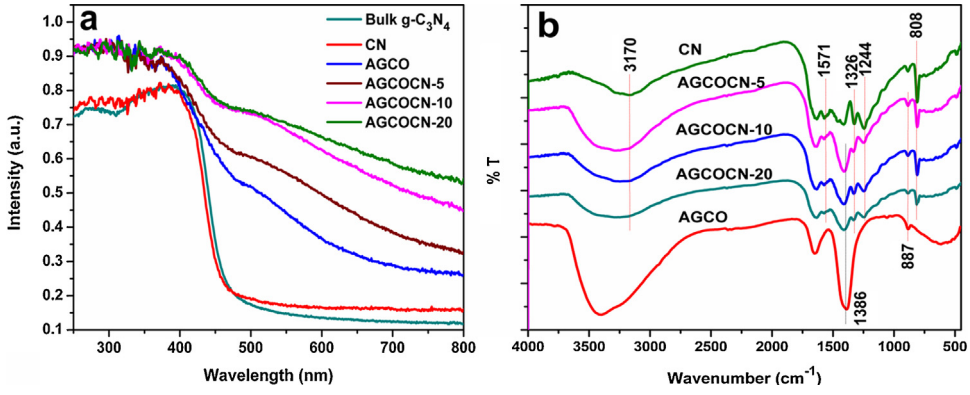

Fig. 2. UV–vis DRS patterns (a) and FT-IR spectra (b) of the synthesized pure Ag_2CO_3, g-C_3N_4 nanosheets and Ag_2CO_3/g-C_3N_4 hetero/nanojunctions.

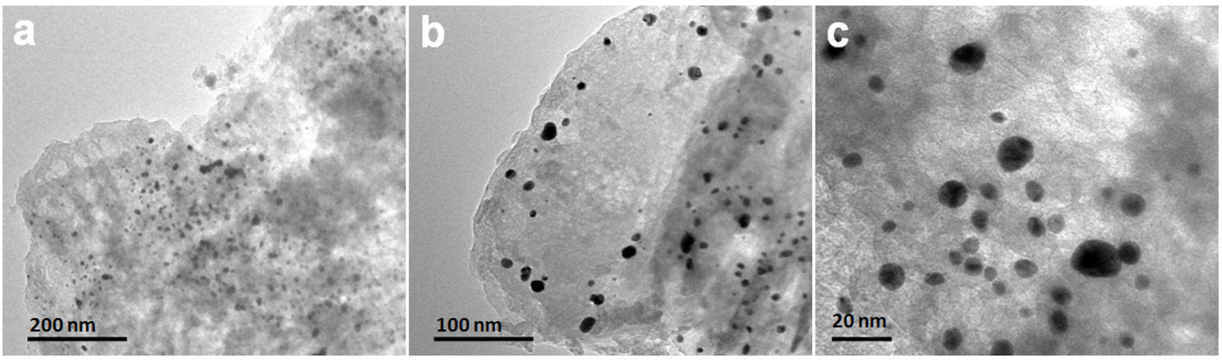

Fig. 3. TEM image (a) and magnified TEM images (b & c) of the synthesized AGCOCN-10 hetero/nanojunction photocatalyst.

NPs were successfully deposited on the surface of the g-C_3N_4 nanosheets by the *in situ* growth mechanism. The size distribution of the Ag_2CO_3 NPs on g-C_3N_4 nanosheets was presented in Fig. S2. The average size of the Ag_2CO_3 NPs was found to be around 15 nm and these NPs were approximately spherical in shape and well dispersed on the g-C_3N_4 surface as shown in Fig. 3c . These results are in good agreement with the XRD observations. In addition, energy dispersive spectroscopy (EDS) was carried out to determine the chemical composition of the synthesized samples. The EDS pattern indicates that the synthesized hetero/nanojunction photocatalyst (AGCOCN-10) was composed of C, N, Ag and O elements as shown in Fig. S3.

The nitrogen adsorption–desorption isotherm analysis was performed to investigate the Brunauer–Emmett–Teller (BET) specific surface area of the synthesized Ag_2CO_3, pure g-C_3N_4 nanosheets and 10 wt% Ag_2CO_3/g-C_3N_4 hetero/nanojunctions. As shown in Fig. 4a, the specific surface area of AGCOCN-10 was found to be 232.78 $m^2 g^{-1}$, which is slightly higher than the CN (224.56 $m^2 g^{-1}$) but much higher than that of AGCO (12.75 $m^2 g^{-1}$). The pore-size distribution analysis of the samples was also estimated using the Barrett–Joyner–Halenda (BJH) method, and results are shown in the inset of Fig. 4a . The pore distribution curves of both CN and AGCOCN-10 samples show narrow and uniform pores with an average pore diameter of 5.8 and 6.6 nm, respectively, which is well consistent with the TEM observation. The large specific surface area and porous structure of Ag_2CO_3/g-C_3N_4 hetero/nanojunctions are useful for the better adsorption of organic compounds and also provide a greater number of reactive sites for the photocatalytic process, thereby enhancing the photocatalytic activity [21,40].

It is widely accepted that the photocatalytic redox reactions are intimately relevant to the separation efficiency of photogenerated electron–hole pairs, which arises from the excited semiconductor materials [41]. To qualitatively investigate the separation efficiency of photogenerated charge carriers during the photocatalytic reactions, the photoluminescence (PL) spectral analysis was performed, which can disclose the migration, transfer, and recombination processes of the photogenerated electron–hole pairs in present hetero/nanojunction system [21]. Fig. 4b shows the PL spectra of the synthesized pure Ag_2CO_3, g-C_3N_4 nanosheets and Ag_2CO_3/g-C_3N_4 hetero/nanojunctions recorded at room temperature with an excitation wavelength of 365 nm. As can be seen from this Figure, the PL spectra of both pure g-C_3N_4 and Ag_2CO_3/g-C_3N_4 hetero/nanojunctions exhibit a strong emission band centered at 460 nm, which can be attributed to the radiative recombination process of self-trapped excitations [42]. Obviously, the intensity of the PL signal for the Ag_2CO_3/g-C_3N_4 hetero/nanojunctions is much lower in comparison with pure g-C_3N_4 and least PL signal observed for AGCOCN-10 photocatalyst. This phenomenon clearly demonstrating that the hetero/nanojunction has a lower recombination rate of photogenerated electron–hole pairs under sunlight irradiation, which is mainly due to the fact that the excited electrons of conduction band from the valence band of g-C_3N_4 are then transfer to Ag_2CO_3, preventing a direct recombination of electron–hole pairs. Thus, the greater separation of photogenerated charge carriers contributes to the enhanced photocatalytic activity of Ag_2CO_3/g-C_3N_4 hetero/nanojunctions [15,43].

To give further evidence to support the above statements, the transient photocurrent response of pure g-C_3N_4, Ag_2CO_3 and Ag_2CO_3/g-C_3N_4 nanocomposite samples were investigated, which

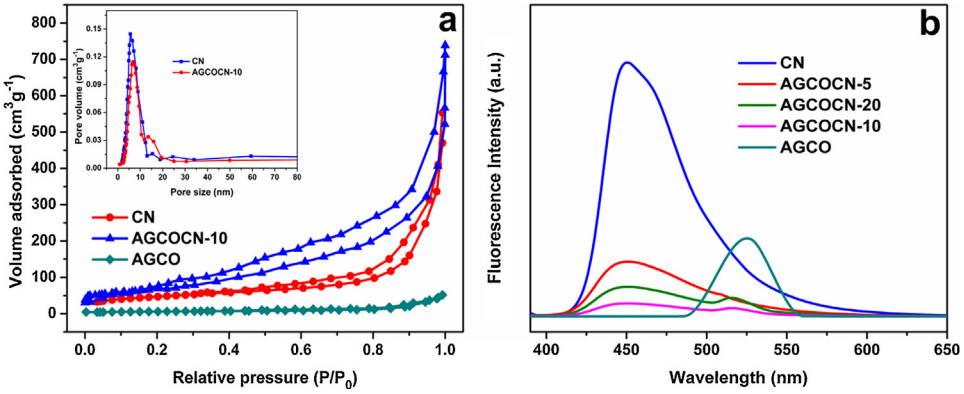

Fig. 4. Nitrogen adsorption–desorption isotherm plots and pore size distribution curves (inset) (a) and room temperature PL spectra (b) of the synthesized pure Ag_2CO_3, g-C_3N_4 nanosheets and Ag_2CO_3/g-C_3N_4 hetero/nanojunction photocatalysts.

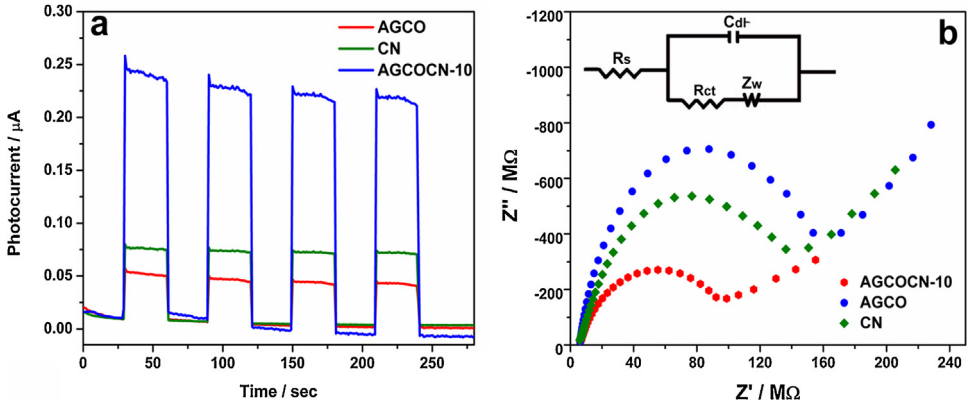

Fig. 5. Photocurrent response (a) and EIS profiles (b) of the synthesized pure Ag_2CO_3, g-C_3N_4 nanosheets and Ag_2CO_3/g-C_3N_4 hetero/nanojunction photocatalysts.

can give the solid evidence to demonstrate the light response and interfacial charge transfer dynamics between the composite semiconductors [24]. Fig. 5a shows the photocurrent-time testing curves of CN, AGCO and AGCOCN-10 photocatalysts with several on–off cycles under visible light irradiation. It can be seen that stable and reproducible photocurrent response to on–off cycles were observed in all three electrodes. Among all photocatalysts, the AGCOCN-10 nanocomposite exhibits a highest photocurrent response, which is much higher than that of CN and AGCO. In general, the photocurrent response of photocatalyst indirectly reflects the ability to generate and transfer the photogenerated charge carrier under light irradiation. From the above discussions we can conclude that the Ag_2CO_3/g-C_3N_4 hetero/nanojunction holds stronger ability in separation of photogenerated electron–hole pairs than g-C_3N_4 and Ag_2CO_3, which is in good agreement with the PL experiments.

EIS measurements were also conducted to investigate the charge transfer resistance and separation efficiency of photogenerated charge carriers in Ag_2CO_3/g-C_3N_4 hetero/nanojunction system. Fig. 5b shows the Nyquist plots of the synthesized CN, AGCO and AGCOCN-10 photocatalysts. The Nyquist plots are best fitted to the equivalent Randle circuit shown in the inset of Fig. 5b. As can be seen from this Figure, the diameter of the semicircle observed for AGCOCN-10 hetero/nanojunction is significantly smaller than that of CN and AGCO. The remarkable decrease in the R_{ct} value of the Ag_2CO_3/g-C_3N_4 hetero/nanojunction photocatalysts clearly demonstrate the enhanced separation efficiency of the photogenerated electron–hole pairs, which can be attributed to the hetero/nanojunction built between g-C_3N_4 and Ag_2CO_3.

Photocatalytic activity of Ag_2CO_3/g-C_3N_4 hetero/nanojunctions

The photocatalytic activity of the synthesized samples was evaluated by photodegradation of the water pollutant, RhB under sunlight irradiation. Fig. 6a shows the variation in concentration of RhB (C/C_0) with irradiation time over pure Ag_2CO_3, g-C_3N_4 nanosheets and Ag_2CO_3/g-C_3N_4 hetero/nanojunctions, where C_0 is the initial concentration of RhB and C is its concentration at time t. For comparison, the photodegradation of RhB over bulk g-C_3N_4 and commercial Degussa P25 was also conducted, which showed poor photocatalytic activity than the other materials. The photocatalytic efficiency of bulk g-C_3N_4 is limited due to the low surface area, high recombination rate of photogenerated charge carriers and limited photo-response range. The photolysis (without catalyst) of the RhB is negligible under same experimental conditions, which confirms that RhB is a stable molecule under sunlight irradiation. Moreover, the adsorption ability of g-C_3N_4 nanosheets and Ag_2CO_3/g-C_3N_4 hetero/nanojunctions was also carried out in the dark for the same duration. The results revealed that the adsorption capacity of these photocatalysts is almost the similar, which indicates that the efficient photogenerated charge separation may be playing an important role in the enhancement of photocatalytic activity. As shown in Fig. 6a, ~99% RhB dye was degraded in 30 min over AGCOCN-10 hetero/nanojunction, whereas 42% and 55% RhB degradation was observed for the same time period in the case of Ag_2CO_3 and g-C_3N_4 nanosheets, respectively. These results clearly demonstrate that the synthesized hetero/nanojunctions exhibited extremely high photocatalytic performance than the Ag_2CO_3 and g-C_3N_4 nanosheets. The photocatalytic

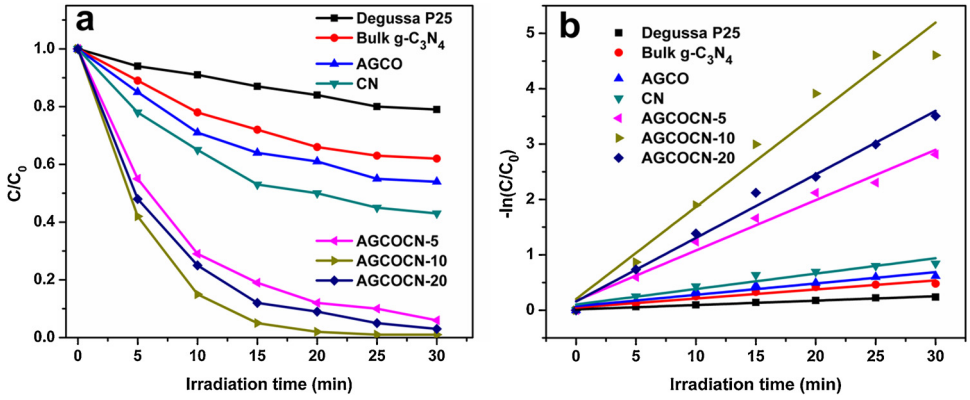

Fig. 6. (a) Comparison of photocatalytic activity for the degradation of RhB under sunlight irradiation over pure Ag_2CO_3, g-C_3N_4 nanosheets and Ag_2CO_3/g-C_3N_4 hetero/nanojunctions and (b) the corresponding first-order kinetics plots of the synthesized pure Ag_2CO_3, g-C_3N_4 nanosheets and Ag_2CO_3/g-C_3N_4 hetero/nanojunction photocatalysts.

degradation efficiency of Ag_2CO_3/g-C_3N_4 hetero/nanojunctions was increased with increasing Ag_2CO_3 NPs content and exhibits optimal photocatalytic efficiency when the loaded Ag_2CO_3 amount was 10 wt%. However, the loaded Ag_2CO_3 NPs content is increased beyond 10 wt%, a decrease in the photocatalytic activity was observed. The decrease in the photocatalytic activity can be explained by following reasons: (1) the optimum Ag_2CO_3 NPs content causes their good dispersion on the surface of g-C_3N_4 nanosheets, which favors the separation and transfer efficiency of the photogenerated charge carriers and (2) at higher Ag_2CO_3 NPs content, there is no strong interfacial charge transfer taking place between isolated Ag_2CO_3 aggregates and g-C_3N_4 nanosheets, which leads to a relatively low charge separation efficiency, and consequently decreasing the photocatalytic activity [44].

The kinetics of RhB photodegradation on the photocatalyst surface can be described by the first-order kinetic equation $\ln(C_0/C) = kt$, where k is the rate constant (min^{-1}). The pseudo first-order rate constants (k) reflect the rate of degradation of RhB over the synthesized photocatalysts under sunlight irradiation. As shown in Fig. 6b, the plot of the irradiation time (t) against $-\ln(C/C_0)$ is nearly a straight line (linear correlation coefficient, $R^2 \geq 0.98$), demonstrating that the photocatalytic degradation curves fit well with the first-order kinetics equation model. The results revealed that the AGCOCN-10 hetero/nanojunction exhibits the highest degradation rate (0.165 min^{-1}), which is almost 5.5 times higher than that of Ag_2CO_3 NPs (0.0298 min^{-1}) and 4 times higher than that of pure g-C_3N_4 nanosheets (0.0389 min^{-1}).

In addition, 4-chlorophenol (4-CP) was chosen as another representative colorless organic pollutant to further evaluate photocatalytic activity of the synthesized samples under sunlight irradiation. As shown in Fig. S4, 4-CP was slightly degraded in absence of catalyst under same experimental conditions, suggesting that the photolysis of 4-CP is negligible. More remarkably, the optimum photocatalytic activity of Ag_2CO_3/g-C_3N_4 hetero/nanojunctions for the photodegradation of 4-CP is much higher than that of pure Ag_2CO_3 and g-C_3N_4 nanosheets. These results clearly demonstrating that the synthesized Ag_2CO_3/g-C_3N_4 hetero/nanojunctions could be a promising visible light photocatalysts not only for colored organic pollutants but also for colorless pollutants under sunlight irradiation.

Mechanism for the enhanced photocatalytic activity and photostability of the Ag_2CO_3/g-C_3N_4 hetero/nanojunctions

In order to understand the photocatalytic mechanism for the synthesized Ag_2CO_3/g-C_3N_4 hetero/nanojunctions in detail, the band edge positions of the conduction band (CB) and valence band (VB) of Ag_2CO_3 and g-C_3N_4 should be determined since they are strongly related to the photocatalytic oxidation process of organic compounds [44,45]. The CB and VB potentials of the semiconductors at the point of zero charge can be calculated according to the following empirical equations:

$$E_{VB} - X - E^e + 0.5Eg \text{ and } E_{CB} - E_{VB} - E_g$$

where X is the absolute electronegativity of the semiconductor, which is the geometric mean of the electronegativity of the constituent atoms, and the value of X for Ag_2CO_3 is *ca.* 6.02 eV; E^e is the energy of free electrons on the hydrogen scale (*ca.* 4.5 eV); E_{CB} and E_{VB} are the CB and VB edge potentials, respectively; and, Eg is the band gap energy of the semiconductor. Based on the above equations, the bottom of the CB and the top of the VB of Ag_2CO_3 are calculated to be +0.36 and +2.68 eV, respectively. Accordingly, the VB and CB of g-C_3N_4 are estimated to be +1.4 and −1.3 eV, respectively.

Detection of reactive species

To explore the photocatalytic mechanism of high photocatalytic activity of the synthesized Ag_2CO_3/g-C_3N_4 hetero/nanojunctions, we first conducted the trapping experiments of main reactive species in this photodegradation process. In general, photogenerated reactive species including superoxide anion radical ($O_2^{\bullet-}$), hydroxyl radical ($^{\bullet}OH$) and holes (h^+) are expected to be involved in the photocatalytic process. To investigate the role of these main reactive species, various scavengers, namely tert-butyl alcohol (TBA) for $^{\bullet}OH$, ammonium oxalate (AO) for holes and N_2 purging for $O_2^{\bullet-}$, were employed in this study [21,27]. As shown in Fig. 7a, the photocatalytic degradation rate was drastically inhibited by the addition of AO, indicating that the photogenerated holes play an important role for the degradation of RhB over Ag_2CO_3/g-C_3N_4 hetero/nanojunctions. When N_2 purging was conducted in the reaction system, the photodegradation of RhB was significantly inhibited, which clearly suggests that the $O_2^{\bullet-}$ are also a predominant active species responsible for the photocatalytic reaction. It is interesting that the conduction band (CB) of Ag_2CO_3 E_{CB} (+0.36 eV *vs.* NHE) is higher than $E(O_2/O_2^{\bullet-})$ (+0.13 eV *vs.* NHE), which cannot produce $O_2^{\bullet-}$ from dissolved O_2 by photogenerated electrons, but the E_{CB} (−1.3 eV *vs.* NHE) of g-C_3N_4 is lower than $E(O_2/O_2^{\bullet-})$, thus the $O_2^{\bullet-}$ species can still be produced in the Ag_2CO_3/g-C_3N_4 hetero/nanojunctions system. However, the degradation efficiency of RhB was not quenched obviously in the presence of TBA, further confirming that the photodegradation of RhB by the present photocatalytic system could mainly be attributed to holes and $O_2^{\bullet-}$ in the whole photocatalytic process under sunlight irradiation.

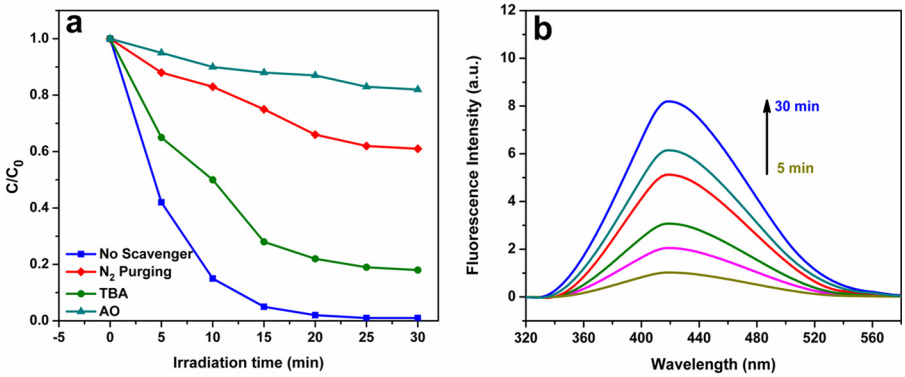

Fig. 7. (a) Effects of different scavengers on the degradation of RhB in presence of AGCOCN-10 photocatalyst under sunlight irradiation and (b) $^{\bullet}OH$ trapping PL spectra of AGCOCN-10 with TA solution under sunlight irradiation.

Hydroxyl radical generation

The •OH generation during the photocatalytic process on the surface of sunlight irradiated photocatalyst was detected by the PL technique using terephthalic acid (TA) as a probe molecule. The •OH readily reacts with TA in basic solution to generate the highly fluorescent product 2-hydroxyterephthalic acid (TAOH). The PL intensity of TAOH was proportional to the amount of •OH radicals generated on the surface of the photocatalysts. A maximum intensity peak in the PL spectra was observed at around 425 nm with an excitation wavelength of 365 nm as shown in Fig. 7b. It can be seen that the PL intensity increases gradually with an increasing irradiation time, which clearly demonstrates that •OH is indeed generated on the sunlight irradiated surface of the Ag_2CO_3/g-C_3N_4 hetero/nanojunctions *via* photocatalytic reactions [33].

Based on the above experimental results, the possible key factors were discussed for the significantly enhanced photocatalytic performance and stability of the synthesized Ag_2CO_3/g-C_3N_4 hetero/nanojunctions. According to the aforementioned calculation results of the band structures, the redox potential of both CB (E_{CB} = −1.3 eV *vs.* NHE) and VB (E_{VB} = +1.4 eV *vs.* NHE) of g-C_3N_4 nanosheets are more negative than those of the CB (E_{CB} = +0.36 eV *vs.* NHE) and VB (E_{VB} = +2.68 eV *vs.* NHE) of Ag_2CO_3, as shown in Fig. 8. Under sunlight irradiation, both g-C_3N_4 and Ag_2CO_3 absorb photons of energy greater than the corresponding band gap energy, which excite the electrons in the VB to the CB and leave holes in the VB. The excited electrons in the CB of the g-C_3N_4 nanosheets can be easily transferred to the CB of the Ag_2CO_3, resulting in accumulation of negative charges in Ag_2CO_3 close to the hetero/nanojunction. At the same time, the hole which was present in the VB of Ag_2CO_3 would transfer to the VB of g-C_3N_4, since band edges of both Ag_2CO_3 and g-C_3N_4 lie in the visible region. The migration of photo-induced charge carriers can be promoted by the inner electric field established at the hetero/nanojunction interface [45]. Therefore, the photogenerated electron–hole pairs will be efficiently separated due to the formation of a hetero/nanojunction between the g-C_3N_4 and Ag_2CO_3 interface, resulting in the enhanced photocatalytic activity of the Ag_2CO_3/g-C_3N_4 photocatalysts. Furthermore, the enriched electrons on the CB of Ag_2CO_3 could be trapped by dissolved oxygen in the reaction solution to form $O_2^{\bullet-}$, which efficiently protects Ag_2CO_3 semiconductor to avoid its photoreduction ($Ag^+ + e- \rightarrow Ag$) [15,46]. As a result, the synthesized photocatalysts exhibit extremely high photostability. Meanwhile, the photogenerated holes on the surface of Ag_2CO_3 migrate to the VB of g-C_3N_4 and react with H_2O to generate •OH. Accordingly, the photogenerated $O_2^{\bullet-}$ and holes followed by •OH can degrade RhB dye and 4-chlorophenol pollutants more efficiently, which is also confirmed by the trapping and •OH radical generation experiments. More importantly, the high specific surface area of Ag_2CO_3/g-C_3N_4 photocatalysts with uniform distribution of Ag_2CO_3 NPs could also account for the enhanced photocatalytic activity of the synthesized Ag_2CO_3/g-C_3N_4 hetero/nanojunctions. All the above aspects together contributed to the enhanced photocatalytic performance and extreme photostability of the Ag_2CO_3/g-C_3N_4 hetero/nanojunction photocatalysts compared to pure Ag_2CO_3 NPs.

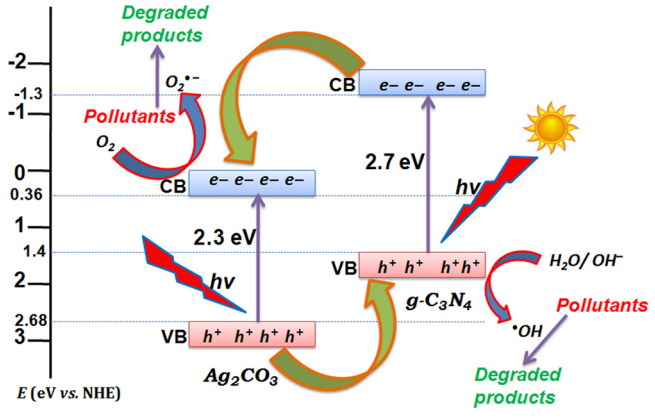

Fig. 8. Schematic photocatalytic reaction process and charge transfer of the Ag_2CO_3/g-C_3N_4 hetero/nanojunctions under sunlight irradiation.

Reusability

The photostability of a photocatalyst is very important characteristic parameter with regard to the practical application [47]. To study the photostability of the synthesized pure Ag_2CO_3 and Ag_2CO_3/g-C_3N_4 hetero/nanojunction, five successive photocatalytic experimental runs were conducted by adding used photocatalyst to fresh RhB solutions with no change in overall concentration of the catalyst under sunlight irradiation. In each recycling run, the photocatalyst was reused after centrifuged, washed with double distilled water and dried at 80 °C while other factors were kept identical. It is well known that an invincible problem for silver-based semiconductor photocatalysts in photocatalysis process is their poor stability under light irradiation [48]. As shown in Fig. 9, the pure Ag_2CO_3 almost lost its activity even in the second run and exhibits very little activity after five successive runs owing to the photocorrosion resulting from the formation of metallic silver [15,21]. More remarkably, the photocatalytic activity of the Ag_2CO_3/g-C_3N_4 photocatalysts was retained at over 90% of its original activity after five successive experimental runs under same conditions, which promotes the photocatalyst for its practical applications in environmental remediation. Figs. S5 and S6 shows the XRD patterns of the synthesized pure Ag_2CO_3 and Ag_2CO_3/g-C_3N_4 photocatalysts after five experimental runs for the degradation of RhB under sunlight irradiation. For pure Ag_2CO_3, it can be seen that a new peak corresponding to Ag^0 appeared together with the XRD peaks of Ag_2CO_3 after the five successive experimental runs, whereas no such peak was observed in the Ag_2CO_3/g-C_3N_4 photocatalysts. These results indicate that Ag_2CO_3 NPs are tightly bound on the surface of the g-C_3N_4 nanosheets through electrostatic interactions, and a strong hetero/nanojunction formed between the Ag_2CO_3 and g-C_3N_4 nanosheets. This hetero/nanojunction can achieve a more efficient charge

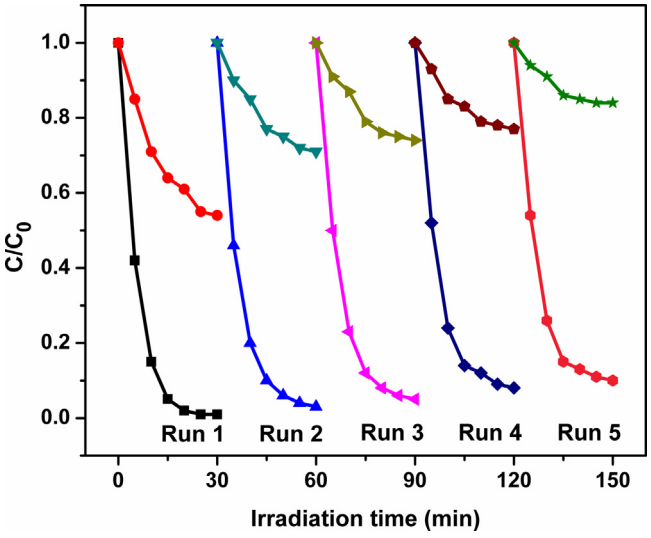

Fig. 9. Reusability of the AGCOCN-10 photocatalyst for the photocatalytic degradation of RhB during five successive experimental runs under sunlight irradiation.

separation and improved lifetime of the charge carriers, which can avoid the reduction of Ag^+ in Ag_2CO_3 by photogenerated electron, and thus inhibited the photocorrosion of Ag_2CO_3 in Ag_2CO_3/g-C_3N_4 photocatalysts during the photocatalytic process.

Conclusion

In summary, highly efficient Ag_2CO_3/g-C_3N_4 hetero/nanojunctions have been successfully fabricated by a facile and template free *in situ* precipitation method. The resulting hetero/nanojunction photocatalysts possess high specific surface area, and strong visible light absorption. More importantly, the synthesized Ag_2CO_3/g-C_3N_4 hetero/nanojunction exhibited the excellent photocatalytic activity for the photocatalytic degradation of RhB and 4-CP, which was superior to those of pure Ag_2CO_3 and g-C_3N_4 nanosheets under sunlight irradiation. Such an enhanced photocatalytic activity could be assigned to the well-established hetero/nanojunction between Ag_2CO_3 and g-C_3N_4 nanosheets, which was favorable for the effective separation of the photogenerated electron–hole pairs. Additionally, the trapping experiments confirmed that photogenerated holes and $O_2^{\bullet-}$ are major responsible for photodegradation in the present hetero/nanojunction system. Furthermore, the hetero/nanojunction improved the photostability of the Ag_2CO_3 NPs on g-C_3N_4 nanosheets. Considering the excellent properties and the facile synthesis procedure, the Ag_2CO_3/g-C_3N_4 hetero/nanojunction may hold great promise as a highly efficient photocatalyst in a wide range of applications including environmental remediation and solar energy applications.

Acknowledgements

Surendar Tonda thanks the Ministry of Human Resource Development, Government of India, for providing a fellowship. The authors also thank Prof. A.K. Ganguli, Indian Institute of Technology Delhi, for carrying out part of this work in his laboratory.

Appendix A. Supplementary data

Supplementary data associated with this article can be found, in the online version, at http://dx.doi.org/10.1016/j.jece.2015.03.021.

References

[1] B. Liu, L.-M. Liu, X.-F. Lang, H.-Y. Wang, X.W. (David) Lou, E.S. Aydil, Doping high-surface-area mesoporous TiO_2 microspheres with carbonate for visible light hydrogen production, Energy Environ. Sci. 7 (8) (2014) 2592–2597, doi:http://dx.doi.org/10.1039/C4EE00472H.
[2] H. Tong, S. Ouyang, Y. Bi, N. Umezawa, M. Oshikiri, J. Ye, Nano-photocatalytic materials: possibilities and challenges, Adv. Mater. 24 (2) (2012) 229–251, doi:http://dx.doi.org/10.1002/adma.201102752. 21972044.
[3] A. Kubacka, M. Fernández-García, G. Colón, Advanced nanoarchitectures for solar photocatalytic applications, Chem. Rev. 112 (3) (2012) 1555–1614, doi:http://dx.doi.org/10.1021/cr100454n. 22107071.
[4] A. Fujishima, K. Honda, Electrochemical photolysis of water at a semiconductor electrode, Nature 238 (5358) (1972) 37–38, doi:http://dx.doi.org/10.1038/238037a0. 12635268.
[5] A.L. Linsebigler, G. Lu, J.T. Yates, Photocatalysis on TiO_2 surfaces: principles, mechanisms, and selected results, Chem. Rev. 95 (3) (1995) 735–758, doi:http://dx.doi.org/10.1021/cr00035a013.
[6] Y. Maruyama, H. Irie, K. Hashimoto, Visible light sensitive photocatalyst, delafossite structured alpha-$AgGaO_2$, J. Phys. Chem. B 110 (46) (2006) 23274–23278, doi:http://dx.doi.org/10.1021/jp063406s. 17107176.
[7] J. Singh, S. Uma, Efficient photocatalytic degradation of organic compounds by ilmenite $AgSbO_3$ under visible and UV light irradiation, J. Phys. Chem. C 113 (28) (2009) 12483–12488, doi:http://dx.doi.org/10.1021/jp901729v.
[8] X. Li, S. Ouyang, N. Kikugawa, J. Ye, Novel Ag_2ZnGeO_4 photocatalyst for dye degradation under visible light irradiation, Appl. Catal. A Gen. 334 (1–2) (2008) 51–58, doi:http://dx.doi.org/10.1016/j.apcata.2007.09.033.
[9] Z. Yi, J. Ye, N. Kikugawa, T. Kako, S. Ouyang, H. Stuart-Williams, et al., An orthophosphate semiconductor with photooxidation properties under visible-light irradiation, Nat. Mater. 9 (7) (2010) 559–564, doi:http://dx.doi.org/10.1038/nmat2780. 20526323.
[10] H. Kato, H. Kobayashi, A. Kudo, Role of Ag^+ in the band structures and photocatalytic properties of $AgMO_3$ (M: Ta and Nb) with the perovskite structure, J. Phys. Chem. B 106 (48) (2002) 12441–12447, doi:http://dx.doi.org/10.1021/jp025974n.
[11] X. Hu, C. Hu, J. Qu, Preparation and visible-light activity of silver vanadate for the degradation of pollutants, Mater. Res. Bull. 43 (11) (2008) 2986–2997, doi:http://dx.doi.org/10.1016/j.materresbull.2007.11.022.
[12] H. Dong, G. Chen, J. Sun, C. Li, Y. Yu, D. Chen, A novel high-efficiency visible-light sensitive Ag_2CO_3 photocatalyst with universal photodegradation performances: simple synthesis, reaction mechanism and first-principles study, Appl. Catal. B. Environ. 134–135 (2013) 46–54, doi:http://dx.doi.org/10.1016/j.apcatb.2012.12.041.
[13] C. Xu, Y. Liu, B. Huang, H. Li, X. Qin, X. Zhang, et al., Preparation, characterization, and photocatalytic properties of silver carbonate, Appl. Surf. Sci. 257 (20) (2011) 8732–8736, doi:http://dx.doi.org/10.1016/j.apsusc.2011.05.060.
[14] G. Dai, J. Yu, G. Liu, A New approach for photocorrosion inhibition of Ag_2CO_3 photocatalyst with highly visible-light-responsive reactivity, J. Phys. Chem. C 116 (29) (2012) 15519–15524, doi:http://dx.doi.org/10.1021/jp305669f.
[15] C. Yu, G. Li, S. Kumar, K. Yang, R. Jin, Phase transformation synthesis of novel Ag_2O/Ag_2CO_3 heterostructures with high visible light efficiency in photocatalytic degradation of pollutants, Adv. Mater. 26 (6) (2014) 892–898, doi:http://dx.doi.org/10.1002/adma.201304173. 24166707.
[16] X. Wang, K. Maeda, A. Thomas, K. Takanabe, G. Xin, J.M. Carlsson, et al., A metal-free polymeric photocatalyst for hydrogen production from water under visible light, Nat. Mater. 8 (1) (2009) 76–80, doi:http://dx.doi.org/10.1038/nmat2317. 18997776.
[17] A. Thomas, A. Fischer, F. Goettmann, M. Antonietti, J.-O. Müller, R. Schlögl, et al., Graphitic carbon nitride materials: variation of structure and morphology and their use as metal-free catalysts, J. Mater. Chem. 18 (41) (2008) 4893–4908, doi:http://dx.doi.org/10.1039/b800274f.
[18] Y. Zhang, J. Liu, G. Wu, W. Chen, Porous graphitic carbon nitride synthesized via direct polymerization of urea for efficient sunlight-driven photocatalytic hydrogen production, Nanoscale 4 (17) (2012) 5300–5303, doi:http://dx.doi.org/10.1039/c2nr30948c. 22776858.
[19] J. Zhang, M. Zhang, R.-Q. Sun, X. Wang, A facile band alignment of polymeric carbon nitride semiconductors to construct isotype heterojunctions, Angew. Chem. Int. Ed. Engl. 51 (40) (2012) 10145–10149, doi:http://dx.doi.org/10.1002/anie.201205333. 22961676.
[20] Y. Zheng, J. Liu, J. Liang, M. Jaroniec, S.Z. Qiao, Graphitic carbon nitride materials: controllable synthesis and applications in fuel cells and photocatalysis, Energy Environ. Sci. 5 (5) (2012) 6717–6731, doi:http://dx.doi.org/10.1039/c2ee03479d.
[21] S. Kumar, T. Surendar, A. Baruah, V. Shanker, Synthesis of a novel and stable g-C_3N_4–Ag_3PO_4 hybrid nanocomposite photocatalyst and study of the photocatalytic activity under visible light irradiation, J. Mater. Chem. A 1 (17) (2013) 5333–5340, doi:http://dx.doi.org/10.1039/c3ta00186e.
[22] A. Suryawanshi, P. Dhanasekaran, D. Mhamane, S. Kelkar, S. Patil, N. Gupta, et al., Doubling of photocatalytic H_2 evolution from g-C_3N_4 via its nanocomposite formation with multiwall carbon nanotubes: electronic and morphological effects, Int. J. Hydrogen Energ. 37 (12) (2012) 9584–9589, doi:http://dx.doi.org/10.1016/j.ijhydene.2012.03.123.
[23] Q. Xiang, J. Yu, M. Jaroniec, Preparation and enhanced visible-light photocatalytic H_2-production activity of graphene/C_3N_4 composites, J. Phys. Chem. C 115 (15) (2011) 7355–7363, doi:http://dx.doi.org/10.1021/jp200953k.
[24] Y. Wang, R. Shi, J. Lin, Y. Zhu, Enhancement of photocurrent and photocatalytic activity of ZnO hybridized with graphite-like C_3N_4, Energy Environ. Sci. 4 (8) (2011) 2922–2929, doi:http://dx.doi.org/10.1039/c0ee00825g.
[25] S. Kumar, T. Surendar, B. Kumar, A. Baruah, V. Shanker, Synthesis of magnetically separable and recyclable g-C_3N_4–Fe_3O_4 hybrid nanocomposites with enhanced photocatalytic performance under visible-light irradiation, J. Phys. Chem. C 117 (49) (2013) 26135–26143, doi:http://dx.doi.org/10.1021/jp409651g.
[26] N. Cheng, J. Tian, Q. Liu, C. Ge, A.H. Qusti, A.M. Asiri, et al., Au-nanoparticle-loaded graphitic carbon nitride nanosheets: green photocatalytic synthesis and application toward the degradation of organic pollutants, A.C.S. Appl. Mater. Interfaces 5 (15) (2013) 6815–6819, doi:http://dx.doi.org/10.1021/am401802r. 23875941.
[27] S. Tonda, S. Kumar, S. Kandula, V. Shanker, Fe-doped and -mediated graphitic carbon nitride nanosheets for enhanced photocatalytic performance under natural sunlight, J. Mater. Chem. A 2 (19) (2014) 6772–6780, doi:http://dx.doi.org/10.1039/c3ta15358d.
[28] H. Zhou, Y. Qu, T. Zeid, X. Duan, Towards highly efficient photocatalysts using semiconductor nanoarchitectures, Energy Environ. Sci. 5 (5) (2012) 6732–6743, doi:http://dx.doi.org/10.1039/c2ee03447f.
[29] L. Sun, X. Zhao, C.-J. Jia, Y. Zhou, X. Cheng, P. Li, et al., Enhanced visible-light photocatalytic activity of g-C_3N_4–$ZnWO_4$ by fabricating a heterojunction: investigation based on experimental and theoretical studies, J. Mater. Chem. 22 (44) (2012) 23428–23438, doi:http://dx.doi.org/10.1039/c2jm34965e.
[30] H.J. Yun, H. Lee, N.D. Kim, D.M. Lee, S. Yu, J. Yi, A combination of two visible-light responsive photocatalysts for achieving the Z-scheme in the solid state,

ACS Nano 5 (5) (2011) 4084–4090, doi:http://dx.doi.org/10.1021/nn2006738. 21500836.
[31] L. Shi, L. Liang, F. Wang, Enhanced visible-light photocatalytic activity and stability over g-C_3N_4/Ag_2CO_3 composites, J. Mater. Sci. 50 (4) (2015) 1718–1727, doi:http://dx.doi.org/10.1007/s10853-014-8733-y.
[32] N. Tian, H. Huang, Y. He, Y. Guo, Y. Zhang, Organic–inorganic hybrid photocatalyst g-C_3N_4/Ag_2CO_3 with highly efficient visible-light-active photocatalytic activity, Colloids Surf. A Physicochem. Eng. Aspects 467 (2015) 188–194, doi:http://dx.doi.org/10.1016/j.colsurfa.2014.11.049.
[33] K. Ishibashi, A. Fujishima, T. Watanabe, K. Hashimoto, Detection of active oxidative species in TiO_2 photocatalysis using the fluorescence technique, Electrochem. Commun. 2 (3) (2000) 207–210, doi:http://dx.doi.org/10.1016/S1388-2481(00)00006-0.
[34] N. Li, G. Liu, C. Zhen, F. Li, L. Zhang, H.-M. Cheng, Battery performance and photocatalytic activity of mesoporous anatase TiO_2 nanospheres/graphene composites by template-free self-assembly, Adv. Funct. Mater. 21 (9) (2011) 1717–1722, doi:http://dx.doi.org/10.1002/adfm.201002295.
[35] S. Ye, L.-G. Qiu, Y.-P. Yuan, Y.-J. Zhu, J. Xia, J.-F. Zhu, Facile fabrication of magnetically separable graphitic carbon nitride photocatalysts with enhanced photocatalytic activity under visible light, J. Mater. Chem. A 1 (9) (2013) 3008–3015, doi:http://dx.doi.org/10.1039/c2ta01069k.
[36] X.-T. Pian, B.-Z. Lin, Y.-L. Chen, J.-D. Kuang, K.-Z. Zhang, L.-M. Fu, Pillared nanocomposite TiO_2/Bi-doped hexaniobate with visible-light photocatalytic activity, J. Phys. Chem. C 115 (14) (2011) 6531–6539, doi:http://dx.doi.org/10.1021/jp1097553.
[37] X. Li, J. Zhang, L. Shen, Y. Ma, W. Lei, Q. Cui, et al., Preparation and characterization of graphitic carbon nitride through pyrolysis of melamine, Appl. Phys. A 94 (2) (2009) 387–392, doi:http://dx.doi.org/10.1007/s00339-008-4816-4.
[38] Y. Song, J. Zhu, H. Xu, C. Wang, Y. Xu, H. Ji, et al., Synthesis, characterization and visible-light photocatalytic performance of Ag_2CO_3 modified by graphene-oxide, J. Alloys Compd. 592 (2014) 258–265, doi:http://dx.doi.org/10.1016/j.jallcom.2013.12.228.
[39] B. Chai, T. Peng, J. Mao, K. Li, L. Zan, Graphitic carbon nitride (g-C_3N_4)-Pt−TiO_2 nanocomposite as an efficient photocatalyst for hydrogen production under visible light irradiation, Phys. Chem. Chem. Phys. 14 (48) (2012) 16745–16752, doi:http://dx.doi.org/10.1039/c2cp42484c. 23138223.
[40] T. Surendar, S. Kumar, V. Shanker, Influence of La-doping on phase transformation and photocatalytic properties of $ZnTiO_3$ nanoparticles synthesized via modified sol–gel method, Phys. Chem. Chem. Phys. 16 (2) (2014) 728–735, doi:http://dx.doi.org/10.1039/c3cp53855a. 24270542.
[41] Y. Zhu, M. Li, Y. Liu, T. Ren, Z. Yuan, Carbon-doped ZnO hybridized homogeneously with graphitic carbon nitride nanocomposites for photocatalysis, J. Phys. Chem. C 118 (20) (2014) 10963–10971, doi:http://dx.doi.org/10.1021/jp502677h.
[42] L. Ge, C. Han, J. Liu, Novel visible light-induced g-C_3N_4/Bi_2WO_6 composite photocatalysts for efficient degradation of methyl orange, Appl. Catal. B. Environ. 108–109 (2011) 100–107, doi:http://dx.doi.org/10.1016/j.apcatb.2011.08.014.
[43] H. Xu, Y. Song, Y. Song, J. Zhu, T. Zhu, C. Liu, et al., Synthesis and characterization of g-C_3N_4/Ag_2CO_3 with enhanced visible-light photocatalytic activity for the degradation of organic pollutants, RSC Adv. 4 (65) (2014) 34539–34547, doi:http://dx.doi.org/10.1039/C4RA03443K.
[44] D. Jiang, J. Zhu, M. Chen, J. Xie, Highly efficient heterojunction photocatalyst based on nanoporous g-C_3N_4 sheets modified by Ag_3PO_4 nanoparticles: synthesis and enhanced photocatalytic activity, J. Colloid Interface Sci. 417 (2014) 115–120, doi:http://dx.doi.org/10.1016/j.jcis.2013.11.042. 24407666.
[45] D. Jiang, L. Chen, J. Zhu, M. Chen, W. Shi, J. Xie, Novel p-n heterojunction photocatalyst constructed by porous graphite-like C_3N_4 and nanostructured BiOI: facile synthesis and enhanced photocatalytic activity, Dalton Trans. 42 (44) (2013) 15726–15734, doi:http://dx.doi.org/10.1039/c3dt52008k. 24051513.
[46] H. Xu, J. Zhu, Y. Song, W. Zhao, Y. Xu, Y. Song, et al., Ion-exchange preparation for visible-light-driven photocatalyst AgBr/Ag_2CO_3 and its photocatalytic activity, RSC Adv. 4 (18) (2014) 9139–9147, doi:http://dx.doi.org/10.1039/c3ra46111d.
[47] S. Kumar, A. Baruah, S. Tonda, B. Kumar, V. Shanker, B. Sreedhar, Cost-effective and eco-friendly synthesis of novel and stable N-doped ZnO/g-C3N4 core-shell nanoplates with excellent visible-light responsive photocatalysis, Nanoscale 6 (9) (2014) 4830–4842, doi:http://dx.doi.org/10.1039/c3nr05271k. 24664127.
[48] C. Dong, K.-L. Wu, X.-W. Wei, X.-Z. Li, L. Liu, T.-H. Ding, et al., Synthesis of graphene oxide–Ag_2CO_3 composites with improved photoactivity and anti-photocorrosion, CrystEngComm 16 (4) (2014) 730–736, doi:http://dx.doi.org/10.1039/C3CE41755G.